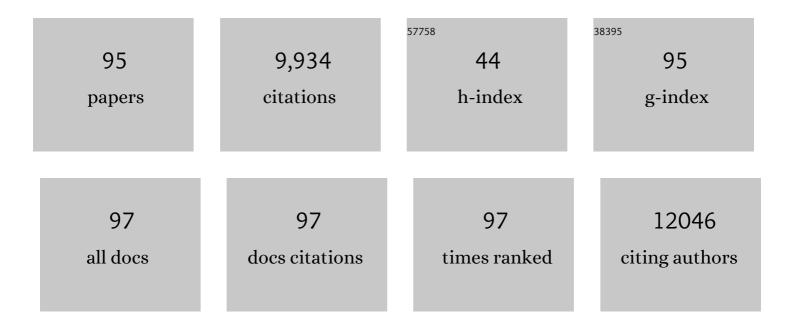
List of Publications by Year in descending order

Source: https://exaly.com/author-pdf/9410094/publications.pdf Version: 2024-02-01



#	Article	IF	CITATIONS
1	CoN4 active sites in locally distorted carbon structure for efficient oxygen reduction reaction via regulating coordination environment. Chemical Engineering Journal, 2022, 429, 132119.	12.7	14
2	Graphitic Carbon Nitride for Photoelectrochemical Detection of Environmental Pollutants. ACS ES&T Engineering, 2022, 2, 140-157.	7.6	41
3	Highly efficient and stable indium single-atom catalysts for electrocatalytic reduction of CO ₂ to formate. Chemical Communications, 2022, 58, 3007-3010.	4.1	23
4	Tuning Active Species in N-Doped Carbon with Fe/Fe ₃ C Nanoparticles for Efficient Oxygen Reduction Reaction. Inorganic Chemistry, 2022, 61, 3166-3175.	4.0	13
5	Accelerating CO ₂ Electroreduction to Multicarbon Products via Synergistic Electric–Thermal Field on Copper Nanoneedles. Journal of the American Chemical Society, 2022, 144, 3039-3049.	13.7	147
6	Ligand Engineering in Nickel Phthalocyanine to Boost the Electrocatalytic Reduction of CO ₂ . Advanced Functional Materials, 2022, 32, .	14.9	80
7	Ultra-thin carbon nitride nanosheets for efficient photocatalytic hydrogen evolution. Chemical Engineering Journal, 2022, 442, 136115.	12.7	48
8	Cu(II)-Grafted Carbon Nitride Quantum Dots with High Crystallinity for Photoelectrochemical Detection Application. Industrial & Engineering Chemistry Research, 2022, 61, 6301-6310.	3.7	10
9	Trash to treasure: Converting red mud into efficient catalysts for the hydrogenation of p-nitrobenzene compounds. Journal of Environmental Chemical Engineering, 2022, 10, 108161.	6.7	3
10	Surface hydroxyl groups functionalized graphite carbon nitride for high efficient removal of diquat dibromide from water. Journal of Colloid and Interface Science, 2021, 582, 70-80.	9.4	32
11	An "on-off-super on―photoelectrochemical sensor based on quenching by Cu-induced surface exciton trapping and signal amplification of copper sulfide/porous carbon nitride heterojunction. Chemosphere, 2021, 267, 129218.	8.2	13
12	Insights into the development of Cu-based photocathodes for carbon dioxide (CO ₂) conversion. Green Chemistry, 2021, 23, 3207-3240.	9.0	26
13	Efficient upcycling electroplating sludge and waste PET into Ni-MOF nanocrystals for the effective photoreduction of CO ₂ . Environmental Science: Nano, 2021, 8, 390-398.	4.3	19
14	Defect-Induced Ce-Doped Bi ₂ WO ₆ for Efficient Electrocatalytic N ₂ Reduction. ACS Applied Materials & Interfaces, 2021, 13, 19864-19872.	8.0	59
15	Tuning Charge Distribution of FeN ₄ via External N for Enhanced Oxygen Reduction Reaction. ACS Catalysis, 2021, 11, 6304-6315.	11.2	114
16	Hydroxyl/amino and Fe(III) co-grafted graphite carbon nitride for photocatalytic removal of volatile organic compounds. Environmental Research, 2021, 197, 111044.	7.5	19
17	Dual Inorganic Sacrificial Template Synthesis of Hierarchically Porous Carbon with Specific N Sites for Efficient Oxygen Reduction. ACS Applied Materials & Interfaces, 2021, 13, 28140-28149.	8.0	12
18	Atomically Dispersed sâ€Block Magnesium Sites for Electroreduction of CO ₂ to CO. Angewandte Chemie, 2021, 133, 25445-25449.	2.0	22

#	Article	IF	CITATIONS
19	Atomically Dispersed sâ€Block Magnesium Sites for Electroreduction of CO ₂ to CO. Angewandte Chemie - International Edition, 2021, 60, 25241-25245.	13.8	104
20	Efficient three-phase electrocatalytic CO ₂ reduction to formate on superhydrophobic Bi–C interfaces. Chemical Communications, 2021, 57, 6011-6014.	4.1	10
21	A highly efficient photoelectrochemical sensor for detection of chlorpyrifos based on 2D/2D β-Bi ₂ O ₃ /g-C ₃ N ₄ heterojunctions. Environmental Science: Nano, 2021, 8, 773-783.	4.3	33
22	Machine Learning in Screening High Performance Electrocatalysts for CO ₂ Reduction. Small Methods, 2021, 5, e2100987.	8.6	60
23	Product selectivity of photocatalytic CO2 reduction reactions. Materials Today, 2020, 32, 222-243.	14.2	719
24	Surfactant-assisted controlled synthesis of a metal-organic framework on Fe2O3 nanorod for boosted photoelectrochemical water oxidation. Chemical Engineering Journal, 2020, 379, 122256.	12.7	64
25	Metallic MoO ₂ â€Modified Graphitic Carbon Nitride Boosting Photocatalytic CO ₂ Reduction via Schottky Junction. Solar Rrl, 2020, 4, 1900416.	5.8	59
26	Co single-atoms on ultrathin N-doped porous carbon <i>via</i> a biomass complexation strategy for high performance metal–air batteries. Journal of Materials Chemistry A, 2020, 8, 2131-2139.	10.3	68
27	Transition Metal Selenides for Electrocatalytic Hydrogen Evolution Reaction. ChemElectroChem, 2020, 7, 31-54.	3.4	103
28	Z‑Scheme cathodic photoelectrochemical sensors for detection of hydrogen sulfide based on AgCl-Ag coupled with porous carbon nitride. Applied Surface Science, 2020, 532, 147424.	6.1	10
29	Modulating Charge Transfer Efficiency of Hematite Photoanode with Hybrid Dualâ€Metal–Organic Frameworks for Boosting Photoelectrochemical Water Oxidation. Advanced Science, 2020, 7, 2002563.	11.2	56
30	Copper Isolated Sites on N-Doped Carbon Nanoframes for Efficient Oxygen Reduction. ACS Sustainable Chemistry and Engineering, 2020, 8, 14030-14038.	6.7	27
31	Bismuth(III)-Doped NaYbF ₄ :Tm ³⁺ Fluorides with Highly Efficient Upconversion Emission under Low Irradiance. Inorganic Chemistry, 2020, 59, 7752-7760.	4.0	8
32	An innovative inÂvitro assay to study the effects of aromatic pollutants on porphyrin systems. Environmental Pollution, 2020, 264, 114606.	7.5	3
33	A regenerative photoelectrochemical sensor based on functional porous carbon nitride for Cu2+ detection. Microchemical Journal, 2020, 156, 104922.	4.5	26
34	Stabilizing CuGaS ₂ by crystalline CdS through an interfacial Z-scheme charge transfer for enhanced photocatalytic CO ₂ reduction under visible light. Nanoscale, 2020, 12, 8693-8700.	5.6	39
35	Plasma-treatment induced H2O dissociation for the enhancement of photocatalytic CO2 reduction to CH4 over graphitic carbon nitride. Applied Surface Science, 2020, 508, 145173.	6.1	44
36	Cobalt Nanoparticles Encapsulated in Nitrogen-Doped Carbon Shells: Efficient and Stable Catalyst for Nitrobenzene Reduction. Industrial & Engineering Chemistry Research, 2020, 59, 4367-4376.	3.7	55

XIAOQING QIU

#	Article	IF	CITATIONS
37	Photoelectrochemical detection of breast cancer biomarker based on hexagonal carbon nitride tubes. Analytical and Bioanalytical Chemistry, 2019, 411, 6889-6897.	3.7	21
38	Graphitic Carbon Nitride with Dopant Induced Charge Localization for Enhanced Photoreduction of CO ₂ to CH ₄ . Advanced Science, 2019, 6, 1900796.	11.2	251
39	Quantum-Dot-Derived Catalysts for CO2 Reduction Reaction. Joule, 2019, 3, 1703-1718.	24.0	106
40	Composition Engineering Boosts Voltage Windows for Advanced Sodium-Ion Batteries. ACS Nano, 2019, 13, 10787-10797.	14.6	90
41	Defect-rich and ultrathin N doped carbon nanosheets as advanced trifunctional metal-free electrocatalysts for the ORR, OER and HER. Energy and Environmental Science, 2019, 12, 322-333.	30.8	1,078
42	Low-temperature route to prepare rare earth fluorides in a molten NH4NO3 system: a systematic study on the effects of NaF/Ln ratio and the reaction temperature and time. CrystEngComm, 2019, 21, 182-189.	2.6	5
43	Oneâ€Pot Synthesis of Novel B, N Co–Doped Carbon Materials for Highâ€Performance Sodiumâ€ion Batteries. ChemistrySelect, 2019, 4, 6445-6450.	1.5	17
44	Plasmonic MoO3-x nanosheets with tunable oxygen vacancies as efficient visible light responsive photocatalyst. Applied Surface Science, 2019, 490, 395-402.	6.1	86
45	In situ synthesis of g-C3N4/TiO2 with {001} and {101} facets coexposed for water remediation. Applied Surface Science, 2019, 487, 322-334.	6.1	27
46	Ag1.69Sb2.27O6.25 coupled carbon nitride photocatalyst with high redox potential for efficient multifunctional environmental applications. Applied Surface Science, 2019, 487, 82-90.	6.1	14
47	Recent advances in different-dimension electrocatalysts for carbon dioxide reduction. Journal of Colloid and Interface Science, 2019, 550, 17-47.	9.4	26
48	Untying thioether bond structures enabled by "voltage-scissors―for stable room temperature sodium–sulfur batteries. Nanoscale, 2019, 11, 5967-5973.	5.6	66
49	In Situ Formation of WO ₃ -Based Heterojunction Photoanodes with Abundant Oxygen Vacancies via a Novel Microbattery Method. ACS Applied Materials & Interfaces, 2019, 11, 15467-15477.	8.0	39
50	Bismuth vanadate single crystal particles modified with tungsten for efficient photoeletrochemical water oxidation. Catalysis Today, 2019, 335, 511-519.	4.4	12
51	A porous carbon nitride modified with cobalt phosphide as an efficient visible-light harvesting nanocomposite for photoelectrochemical enzymatic sensing of glucose. Mikrochimica Acta, 2019, 186, 856.	5.0	10
52	Enhancement of photocatalytic activities in hierarchical BiOBr microï¬,owers induced by oxygen vacancies. Catalysis Today, 2019, 335, 193-199.	4.4	58
53	Chemoselective hydrogenation of nitrobenzenes activated with tuned Au/h-BN. Journal of Catalysis, 2019, 370, 55-60.	6.2	48
54	Solution evaporation processed high quality perovskite films. Science Bulletin, 2018, 63, 1591-1596.	9.0	34

#	Article	IF	CITATIONS
55	Nanorod-assembled NiCo ₂ O ₄ hollow microspheres assisted by an ionic liquid as advanced electrode materials for supercapacitors. RSC Advances, 2017, 7, 11123-11128.	3.6	26
56	High-rate sodium ion anodes assisted by N-doped carbon sheets. Sustainable Energy and Fuels, 2017, 1, 1130-1136.	4.9	23
57	Magnetically recyclable Ni@h-BN composites for efficient hydrolysis of ammonia borane. International Journal of Hydrogen Energy, 2017, 42, 16003-16011.	7.1	46
58	Oxygen Vacancies Evoked Blue TiO ₂ (B) Nanobelts with Efficiency Enhancement in Sodium Storage Behaviors. Advanced Functional Materials, 2017, 27, 1700856.	14.9	212
59	Enhanced stability and catalytic activity of bismuth nanoparticles by modified with porous silica. Journal of Physics and Chemistry of Solids, 2017, 110, 9-14.	4.0	22
60	Hollow-sphere ZnSe wrapped around carbon particles as a cycle-stable and high-rate anode material for reversible Li-ion batteries. New Journal of Chemistry, 2017, 41, 6693-6699.	2.8	40
61	Carbon Anode Materials for Advanced Sodiumâ€lon Batteries. Advanced Energy Materials, 2017, 7, 1602898.	19.5	858
62	Constructing hierarchical sulfur-doped nitrogenous carbon nanosheets for sodium-ion storage. Nanotechnology, 2017, 28, 445604.	2.6	13
63	Antimony Anchored with Nitrogen-Doping Porous Carbon as a High-Performance Anode Material for Na-Ion Batteries. ACS Applied Materials & Interfaces, 2017, 9, 26118-26125.	8.0	55
64	Nanoâ€confined Mo ₂ C Particles Embedded in a Porous Carbon Matrix: A Promising Anode for Ultraâ€stable Na Storage. ChemElectroChem, 2017, 4, 2669-2676.	3.4	17
65	One-step synthesis of magnetically recyclable Co@BN core–shell nanocatalysts for catalytic reduction of nitroarenes. RSC Advances, 2017, 7, 35451-35459.	3.6	29
66	Layerâ€Tunable Phosphorene Modulated by the Cation Insertion Rate as a Sodiumâ€Storage Anode. Advanced Materials, 2017, 29, 1702372.	21.0	162
67	Controllable Interlayer Spacing of Sulfurâ€Doped Graphitic Carbon Nanosheets for Fast Sodiumâ€lon Batteries. Small, 2017, 13, 1700762.	10.0	144
68	Visible light photocatalytic activity induced by Rh(III) modification on the surface of BiOCl. Applied Surface Science, 2016, 387, 45-50.	6.1	38
69	The release of hydrogen from ammonia borane over copper/hexagonal boron nitride composites. RSC Advances, 2016, 6, 106211-106217.	3.6	31
70	Hydrogenation of nitroarenes into aromatic amines over Ag@BCN colloidal catalysts. Journal of Colloid and Interface Science, 2016, 477, 131-137.	9.4	25
71	Visible-Light-Sensitive Photocatalysts: Nanocluster-Grafted Titanium Dioxide for Indoor Environmental Remediation. Journal of Physical Chemistry Letters, 2016, 7, 75-84.	4.6	138
72	Boron nitride encapsulated copper nanoparticles: a facile one-step synthesis and their effect on thermal decomposition of ammonium perchlorate. Scientific Reports, 2015, 5, 16736.	3.3	46

#	Article	IF	CITATIONS
73	Electronic structure and photocatalytic activities of (Bi2â^Y)Sn2O7 solid solution. Applied Surface Science, 2015, 357, 2364-2371.	6.1	9
74	Hierarchical BiOCl microflowers with improved visible-light-driven photocatalytic activity by Fe(III) modification. Applied Catalysis B: Environmental, 2015, 174-175, 105-112.	20.2	155
75	Porous cubic bismuth oxide nanospheres: A facile synthesis and their conversion to bismuth during the reduction of nitrobenzenes. Chemical Engineering Science, 2015, 131, 155-161.	3.8	28
76	Mesoporous Iron Trifluoride Microspheres as Cathode Materials for Li-ion Batteries. Electrochimica Acta, 2015, 151, 355-362.	5.2	22
77	Iodine Modified Carbon Nitride Semiconductors as Visible Light Photocatalysts for Hydrogen Evolution. Advanced Materials, 2014, 26, 805-809.	21.0	1,033
78	Cu(<scp>ii</scp>) nanocluster-grafted, Nb-doped TiO ₂ as an efficient visible-light-sensitive photocatalyst based on energy-level matching between surface and bulk states. Journal of Materials Chemistry A, 2014, 2, 13571-13579.	10.3	49
79	A facile one-pot synthesis of Cu–Cu ₂ O concave cube hybrid architectures. CrystEngComm, 2014, 16, 4967-4972.	2.6	25
80	Dispersed Cu ₂ 0 Octahedrons on h-BN Nanosheets for <i>p</i> -Nitrophenol Reduction. ACS Applied Materials & Interfaces, 2014, 6, 14469-14476.	8.0	234
81	Insights into the photosensitivity activity of BiOCl under visible light irradiation. Applied Catalysis B: Environmental, 2014, 158-159, 182-189.	20.2	181
82	Enhanced Photoactivity with Nanocluster-Grafted Titanium Dioxide Photocatalysts. ACS Nano, 2014, 8, 7229-7238.	14.6	120
83	Stable colloidal boron nitride nanosheet dispersion and its potential application in catalysis. Journal of Materials Chemistry A, 2013, 1, 12192.	10.3	151
84	Enhanced photocatalytic activity of Bi2O3 under visible light irradiation by Cu(II) clusters modification. Applied Catalysis B: Environmental, 2013, 142-143, 598-603.	20.2	118
85	Energy-Level Matching of Fe(III) Ions Grafted at Surface and Doped in Bulk for Efficient Visible-Light Photocatalysts. Journal of the American Chemical Society, 2013, 135, 10064-10072.	13.7	263
86	Hybrid Cu _{<i>x</i>} O/TiO ₂ Nanocomposites As Risk-Reduction Materials in Indoor Environments. ACS Nano, 2012, 6, 1609-1618.	14.6	387
87	Reaction mechanism of visible-light responsive Cu(II)-grafted Mo-doped SrTiO3 photocatalyst studied by means of ESR spectroscopy and chemiluminescence photometry. Applied Catalysis B: Environmental, 2012, 111-112, 636-640.	20.2	30
88	Cu(II) Oxide Amorphous Nanoclusters Grafted Ti ³⁺ Self-Doped TiO ₂ : An Efficient Visible Light Photocatalyst. Chemistry of Materials, 2011, 23, 5282-5286.	6.7	262
89	Visible-Light-Driven Cu(II)â^'(Sr _{1â^'<i>y</i>} Na _{<i>y</i>})(Ti _{1â^'<i>x</i>} Mo _{<i>x</i>} Photocatalysts Based on Conduction Band Control and Surface Ion Modification. Journal of the American Chemical Society. 2010. 132. 15259-15267.)O _{3 13.7}	3 197
90	ZnO Twin-Cones: Synthesis, Photoluminescence, and Catalytic Decomposition of Ammonium Perchlorate. Inorganic Chemistry, 2008, 47, 4146-4152.	4.0	131

#	Article	IF	CITATIONS
91	Origin of the Enhanced Photocatalytic Activities of Semiconductors: A Case Study of ZnO Doped with Mg ²⁺ . Journal of Physical Chemistry C, 2008, 112, 12242-12248.	3.1	229
92	Doping effects of Co ²⁺ ions on ZnO nanorods and their photocatalytic properties. Nanotechnology, 2008, 19, 215703.	2.6	104
93	Inheriting morphology and photoluminescence properties of MgO nanoplates. Journal of Materials Research, 2007, 22, 908-912.	2.6	12
94	Nature of the abnormal band gap narrowing in highly crystalline Zn1â^'xCoxO nanorods. Applied Physics Letters, 2006, 88, 114103.	3.3	56
95	Correlation between size-induced lattice variations and yellow emission shift in ZnO nanostructures. Applied Physics Letters, 2005, 87, 124101.	3.3	42